Br J Clin Pharmacol 1996; **41**: 593–604

Enzyme kinetic modelling as a tool to analyse the behaviour of cytochrome P450 catalysed reactions: application to amitriptyline *N*-demethylation

JÜRGEN SCHMIDER, DAVID J. GREENBLATT, JEROLD S. HARMATZ & RICHARD I. SHADER
Department of Pharmacology and Experimental Therapeutics, Tufts University School of Medicine, Boston, MA, USA

1 To determine kinetic parameters (V_{max}, K_m) for cytochrome P450 (CYP) mediated metabolic pathways, nonlinear least squares regression is commonly used to fit a model equation (e.g., Michaelis Menten [MM]) to sets of data points (reaction velocity *vs* substrate concentration). This method can also be utilized to determine the parameters for more complex mechanisms involving allosteric or multi-enzyme systems. Akaike's Information Criterion (AIC), or an estimation of improvement of fit as successive parameters are introduced in the model (*F*-test), can be used to determine whether application of more complex models is helpful. To evaluate these approaches, we have examined the complex enzyme kinetics of amitriptyline (AMI) *N*-demethylation *in vitro* by human liver microsomes.

2 For a 15-point nortriptyline (NT) formation rate *vs* substrate (AMI) concentration curve, a two enzyme model, consisting of one enzyme with MM kinetics ($V_{max} = 1.2$ nmol min^{-1} mg^{-1}, $K_m = 24$ μM) together with a sigmoidal component (described by an equation equivalent to the Hill equation for cooperative substrate binding; $V_{max} = 2.1$ nmol min^{-1} mg^{-1}, $K' = 70$ μM; Hill exponent $n = 2.34$), was favoured according to AIC and the *F*-test.

3 Data generated by incubating AMI under the same conditions but in the presence of 10 μM ketoconazole (KET), a CYP3A3/4 inhibitor, were consistent with a single enzyme model with substrate inhibition ($V_{max} = 0.74$ nmol min^{-1} mg^{-1}, $K_m = 186$ μM, $K_1 = 0.0028$ μM^{-1}).

4 Sulphaphenazole (SPA), a CYP2C9 inhibitor, decreased the rate of NT formation in a concentration dependent manner, whereas a polyclonal rat liver CYP2C11 antibody, inhibitory for S-mephenytoin 4′-hydroxylation in humans, had no important effect on this reaction.

5 Incubation of AMI with 50 μM SPA resulted in a curve consistent with a two enzyme model, one with MM kinetics ($V_{max} = 0.72$ nmol min^{-1} mg^{-1}, $K_m = 54$ μM) the other with 'Hill-kinetics' ($V_{max} = 2.1$ nmol min^{-1} mg^{-1}, $K' = 195$ μM; $n = 2.38$).

6 A fourth data-set was generated by incubating AMI with 10 μM KET and 50 μM SPA. The proposed model of best fit describes two activities, one obeying MM-kinetics ($V_{max} = 0.048$ nmol min^{-1} mg^{-1}, $K_m = 7$ μM) and the other obeying MM kinetics but with substrate inhibition ($V_{max} = 0.8$ nmol min^{-1} mg^{-1}, $K_m = 443$ μM, $K_1 = 0.0041$ μM^{-1}).

7 The combination of kinetic modelling tools and biological data has permitted the discrimination of at least three CYP enzymes involved in AMI *N*-demethylation. Two are identified as CYP3A3/4 and CYP2C9, although further work in several more livers is required to confirm the participation of the latter.

Correspondence: Dr Jürgen Schmider, Department of Pharmacology and Experimental Therapeutics, Tufts University School of Medicine, 136 Harrison Avenue, Boston, MA 02111, USA

Keywords cytochrome P450 amitriptyline enzyme kinetics Michaelis Menten equation Akaike's Information Criterion nonlinear regression

Introduction

The biotransformation of many drugs is mediated by cytochrome (CYP) isoforms. The primary site of these metabolic transformations is the smooth endoplasmic reticulum of the liver, although several other tissues have been shown to express CYP isoforms [1–4]. Using microsomal preparations of human liver tissue, the enzyme kinetics of individual metabolic pathways can be characterised [5–9]. Enzymatic activity is typically expressed in the form of the kinetic parameters V_{max} (maximal formation rate) and K_m (Michaelis constant) which are estimated by measuring product formation rates under initial rate conditions over a range of substrate concentrations. Computers facilitate fitting model rate-equations directly to these data points and eliminate the necessity of transforming data via reciprocal equations. Such transformations may introduce problems associated with distortion of error terms and exaggeration of small values [10]. Specifically, nonlinear regression also allows fitting of experimental data to model equations associated with more complex mechanisms involving allosteric and/or multi-enzyme systems.

In many cases the investigator is primarly interested in deriving inhibition constants, and accurate modelling of formation rates is not of major concern. The most commonly used approach is to employ a Michaelis Menten (MM) equation with formation rate data, from which inhibition constants are readily derived. This approach does not require many data points since only three parameters are iterated, namely V_{max}, K_m and K_1 (inhibition constant).

We have recently established that the *N*-demethylation of amitriptyline (AMI) is mediated by at least two enzymes *in vitro* [5], one of which is CYP3A3/4. Even though only eight data points were used, it was evident that NT-formation rates were better fitted by a model describing allosteric behavior of the enzyme (Hill-equation). This finding led us to investigate whether enzyme kinetic modelling could be used to explore complex metabolic mechanisms as applied to amitriptyline (AMI) *N*-demethylation in a representative human liver sample. Clearly the selection of a model to explain a particular set of data will not be based entirely on numerical considerations. Of central importance is the biochemical plausibility of the model, as well as its consistency with other biological evidence [10].

The use of more complex model equations requires additional iterated parameters which typically improve the goodness of fit [10]. Two methods are commonly applied to assess the fit of more complex models: 1) the *F*-test, which evaluates the statistical significance of any improvement produced by the introduction of an additional parameter [10, 11]; and 2) Akaike's Information Criterion (AIC), a numeric index reflecting the information value of adding further parameters [12, 13].

To elucidate the complex metabolic mechanisms of AMI *N*-demethylation we applied a sequence of model equations of increasing complexity and number of parameters to a 15-point nortriptyline (NT) formation rate *vs* AMI concentration curve. In addition we evaluated these models of NT formation in the presence of chemical inhibitors and an inhibitory antibody.

Methods

Chemicals

AMI and NT were purchased from Sigma, St Louis, MO. Sulphaphenazole (SPA) was from RBI, Natick, MA. Ketoconazole (KET) was kindly provided by the Janssen Research Foundation, Beerse, Belgium. The cofactors NADP, (±)-isocitric acid, $MgCl_2$, and isocitrate dehydrogenase were from Sigma, as was the potassium phosphate salt used in buffer solution. All organic solvents were of reagent grade.

Source of human liver sample and preparation of microsomes

The liver sample, obtained from the International Institute for the Advancement of Medicine (Exton, PA, USA), was from a transplant donor without known liver disease. The tissue was partitioned and kept at −80° C until the time of microsome preparation, as described previously [14, 15].

The protein concentration in the microsome sample was determined using the Bicinchoninic Acid Protein Assay (BCA-Pierce). Bovine serum albumin was used as standard.

Enzyme activities for index reactions reflecting CYP1A1/2, CYP2D6, CYP2C9, CYP2C19, CYP2E1 and CYP3A3/4 for this liver are reported elsewhere [6].

Source of antibody

The polyclonal rabbit-derived rat liver CYP3A1 antibody serum and the rabbit control serum were purchased from Human Biologics, Inc., Phoenix, Arizona [6, 16]. The polyclonal goat anti-rat liver CYP2C11 antibody serum and the control goat serum were from Gentest Corporation, Woburn, MA, USA [6].

Incubation condititions

Enzyme kinetic and chemical inhibitor studies Incubation mixtures contained 50 mM potassium phosphate buffer (pH adjusted to 7.5 at 25° C). AMI

(2.5–500 μM), 0.5 mM NADP, 3.75 mM (±)-isocitric acid, 1 unit ml^{-1} of isocitrate dehydrogenase and 5 mM Mg^{2+} in the presence or absence of KET (10 μM) and/or SPA (50 μM). Incubation mixtures with SPA (1–100 μM) contained a fixed concentration of AMI (100 μM). Final volumes were 250 μl, with a microsomal protein concentration of 200 μg ml^{-1}. Solutions of AMI, NT and the inhibitors were prepared in methanol. The solvent was evaporated to dryness prior to addition of cofactors.

Substrate, inhibitors, incubation buffer, and cofactors were preincubated at 37° C for 5 min, and reactions were initiated by the addition of microsomes. Incubations were performed for 20 min at 37° C, and stopped by the addition of 50 μl of 1 *N* hydrochloric acid and cooling on ice. Desipramine was then added as an internal standard, and the mixture was spun at 16000 *g* for 5 min in a Micro-MB centrifuge. Supernatants were injected into the h.p.l.c. All incubations were performed in duplicate.

Immunoinhibition studies Using the same incubation buffer as described above, microsomes and either antibody serum or control serum were preincubated at 37° C for 20 min with 100 μM AMI. Reactions were then initiated by the addition of the cofactors to a final volume of 250 μl. Incubations were performed for 20 min at 37° C, and the incubation mixtures processed as described above. Owing to limited antibody availability, only single incubations were performed.

Analysis of nortriptyline by h.p.l.c.

Concentrations of NT were determined using h.p.l.c. with ultraviolet detection (Waters Associates, Milford, MA). A 30 cm × 3.9 mm steel C_{18} μBondapack column and a Lambda-Max Model 480 LC ultraviolet spectrophotometer, set at a wavelength of 220 nm, were used. The mobile phase consisted of 35% acetonitrile and 65% 50 mM potassium phosphate buffer (pH 6) and run at a flow rate of 1.4 ml min^{-1}. Standard curves were prepared by adding incubation buffer and internal standard (desipramine) to known amounts of NT, yielding a final volume of 250 μl. The inhibitors KET and SPA did not interfere with the assays. The between-day coefficient of variation for identical samples (left for 36 h at room temperature) was less than 3%. Chromatograms were analyzed by measuring peak height utilizing the internal standard method. The limit of detection was 0.05 nmol NT for each incubation sample. Average coefficient of variation for duplicate standard curve data points was 3.42% (range 0–8%), and for control curve data points 4.46% (range 0.3–15%). The coefficient of variation of six identical samples at 0.1 nmol NT was 5.24%, at 1 nmol was 3.82%, and at 10 nmol was 1.6%.

Identification of metabolites

Incubations without microsomes were used to verify that formation of the observed metabolic products required microsomal enzymes. The identity of NT was verified by comparing its retention time with that of an authentic standard.

Data analysis

All reaction velocities were based on a 20 min incubation, which falls within the linear time period of the reaction and allows the assumption of initial rate conditions. Rates were expressed in $nmol^{-1}min^{-1}mg$ protein. The mean of duplicate data points consisting of NT reaction velocities (v) at varying concentrations of the substrate AMI (S) with or without the inhibitor KET were fitted without weighting by derivative-free iterative nonlinear least-squares regression [17] to the following equations:

—a one enzyme model MM equation (two parameters):

$$v = V_{max} \cdot S/(K_m + S) \quad (1)$$

—a one enzyme model Hill equation (three parameters):

$$v = V_{max} \cdot S^n/(K'^n + S^n) \quad (2)$$

—a one enzyme MM model with substrate inhibition (three parameters):

$$v = V_{max} \cdot S/(K_m + S + 1/K_1 \cdot S^2) \quad (3)$$

—a two enzyme model, both MM (four parameters):

$$v = V_{max(1)} \cdot S/(K_{m(1)} + S) + V_{max(2)} \cdot S/(K_{m(2)} + S) \quad (4)$$

—a two enzyme model consisting of a MM and a Hill equation (five parameters):

$$v = V_{max(1)} \cdot S/(K_m + S) + V_{max(2)} \cdot S^n/(K'^n + S^n) \quad (5)$$

—a two enzyme model consisting of a MM and a MM equation with substrate inhibition (five parameters):

$$v = V_{max(1)} \cdot S/(K_{m(1)} + S) + V_{max(2)} \cdot S/(K_{m(2)} + S + K_1 \cdot S^2) \quad (6)$$

—a two enzyme model consisting of two Hill equations (six parameters):

$$v = V_{max(1)} \cdot S^{n(1)}/({K'_{(1)}}^{n(1)} + S^{n(1)}) + V_{max(2)} \cdot S^{n(2)}/({K'_{(2)}}^{n(2)} + S^{n(2)}) \quad (7)$$

—a two enzyme model consisting of a Hill equation and a MM equation with substrate inhibition (six parameters):

$$v = V_{max(1)} \cdot S/(K_m + S + K_1 \cdot S^2) + V_{max(2)} \cdot S^n/(K'^n + S^n) \quad (8)$$

$K_{m(1)}$ is the substrate concentration at which the reaction velocity is 50% of $V_{max(1)}$. K_1 [18] is a constant indicating the degree of substrate inhibition and is equal to $1/K_{IS}$ [19]. n(i) is equivalent to the Hill-coefficient for cooperative substrate binding. K' [20] is the substrate concentration at which the reaction velocity

equals 50% of V_{max} and is therefore equivalent to K_m derived by the MM equation. The combination of two enzymes with substrate inhibition did not yield a convergent solution for any dataset. For all models (except equation 4, which did not provide improvement in the sum of squared residuals for any dataset), an *F*-test was performed and the AIC applied. Starting with the equation with the fewest parameters (equation 1), the equation with the next higher number of parameters was applied, as long as goodness of fit continued to improve as indicated by AIC and the *F*-test.

Immunoinhibition data were expressed as the percentage of the formation rate in the presence of antibodies or control serum of that of the formation rate without antibodies.

Results

The Eadie-Hofstee plot of NT formation rate without inhibitor displayed a slight outward (convex) curvature (Figure 1b). Nevertheless the plot of reaction velocity *vs* substrate concentration did not show a sigmoid shape for the very low substrate concentrations (2.5 to 25 μM; Figure 1a, insert). Fitting these data points with equations 1–6, the two enzyme model consisting of a MM and Hill equation (five parameter model) fitted better than the three parameter models, whereas the two six-parameter models provided no further improvement in goodness of fit (*F*-test; Table 1). Fitting equation 6 to the obtained data points did not yield a convergent solution. Equation 5 was also favored by AIC (smallest value; Table 1). In the plot of normalized residuals (ratio of residual over predicted value) *vs* predicted values (Figure 2), equations 1–4 do not appear to form a randomized horizontal band of points, whereas equations 5, 7, and 8 produced residuals that are more evenly scattered.

The formation of NT in the presence of 10 μM ketoconazole was consistent with a model of substrate inhibition according to the velocity-plot and the Eadie-Hofstee plot (Figures 3a, b). Statistical analysis of the fitted parameters obtained from equations 1 to 5 (equations 6, 7, and 8 did not converge) also supported the use of this model (Table 2). However, the residuals generated by equation 3 were only approximately random (Figure 4).

The polyclonal rat liver CYP2C11 antibody, which specifically inhibits S-mephenytoin 4′-hydroxylation and to a lesser extent phenytoin 4-hydroxylation in human microsomes [6], produced no significant inhibition of AMI *N*-demethylation. However, SPA, a specific CYP2C9 inhibitor, decreased NT formation in a concentration dependent manner (Figure 5).

The Eadie-Hofstee plot of NT formation in presence of 50 μM SPA (Figure 6b) displayed a biphasic pattern with a low affinity component exhibiting a convex curvature and a linear high affinity component. The *F*-test as well as AIC suggested a two enzyme model consisting of a MM and Hill equation (equation 5; Table 3). Fitting equations 3 and 6 to the obtained data points did not yield a convergent solution. Although the plot of normalized residuals *vs* predicted values (Figure 7), did not result in an ideal horizontal scattering of the data points, equation 5 appeared to be superior compared to equations 1–4 and similar to equations 7 and 8.

Adding fixed concentrations of 10 μM KET and 50 μM SPA to varying AMI concentrations revealed an Eadie-Hofstee plot which also displayed a slight biphasic pattern (Figure 8b). There was a low-affinity component consistent with a model of substrate inhibition along with an equivocal high-affinity site. According to the

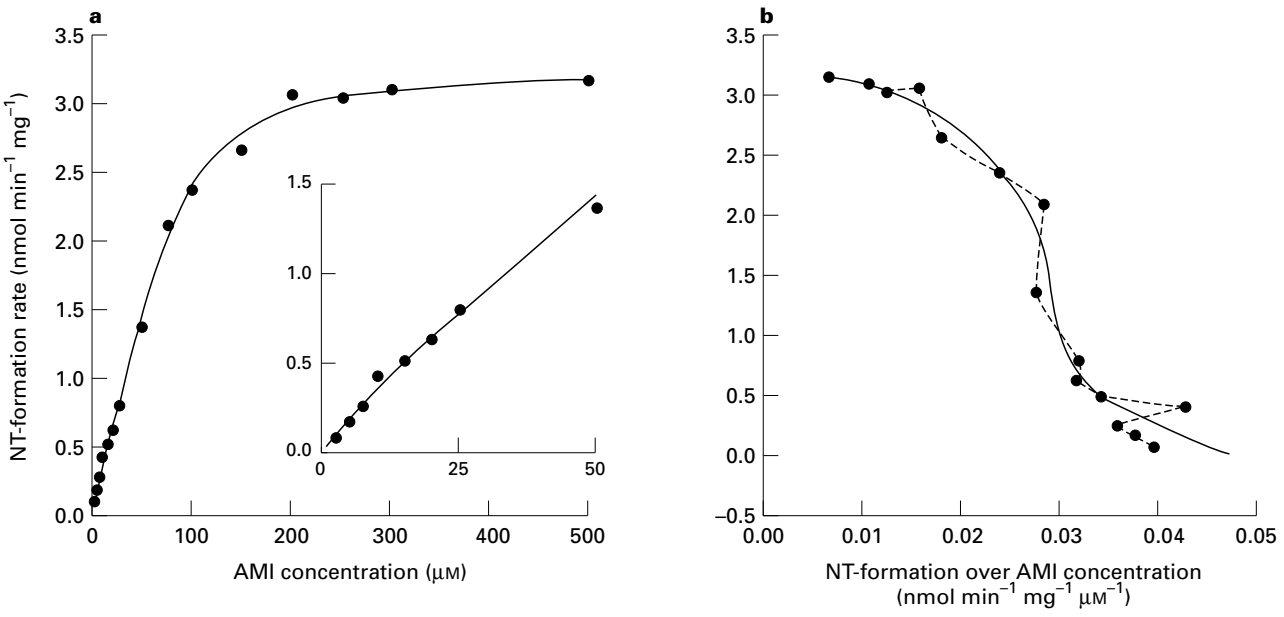

Figure 1 Plot of NT-formation rate *vs* AMI concentration (a) and Eadie-Hofstee plot (b) for uninhibited NT-formation rates. The solid line in both graphs represents the curve of best fit as iterated with equation 5. The broken line joins the points with respect to increasing substrate concentration. Insert: magnification of the graph at low AMI concentrations.

Table 1 Kinetic parameters and statistical evaluation of NT formation without inhibitor

Model	V_{max}[a]	K_m[a]; K'[a]	n[a]; K_1[a]	V_{max}[b]	K_m[b]; K'[b]	n[b]; K_1[b]	*AIC*[c]	*Comp.*[d]	F[e]	$F_{\{0.05\}}$[f]
Eq. 1	4.0	80					−14.5	Eq. 2	18.0	4.75
								Eq. 3	26.3	4.75
CV[g]	4.2	12								
Eq. 2	3.4	58	1.35				−26.2	Eq. 5	6.6	4.1
CV[g]	3.3	7.9	7							
Eq. 3	5.9	146	0.0012				−29.9	Eq. 5	4.1	4.1
CV[g]	10.8	17	31							
Eq. 4	0.8	80		3.1	80		−10.5			
CV[g]	$>10^6$	$>10^6$		$>10^6$	$>10^6$					
Eq. 5	1.2	24		2.1	70	2.3	−34.8	Eq. 7	0.3	5.12
								Eq. 8	0.03	5.12
CV[g]	143	182		76	8.9	43				
Eq. 7	0.5	7.3	1.7	2.7	68	2.11	−33.4			
CV[g]	80	98	82	18	12	18				
Eq. 8	1.1	23.3	0.0001	2.2	71	2.25	−32.9			
CV[g]	164	206	566	83	13	47				

Equation 6 did not yield a convergent solution. Equation 4 was not included in the comparison with the *F*-test because it provided values for the sum of squared residuals which were identical as for equation 1. V_{max} in nmol min^{-1} mg^{-1} protein; K_m, K' in μM; K_1 in μM^{-1}; n arbitrary units; [a]: first enzyme; [b]: second enzyme; [c]: Akaike's information criterion; [d]: comparison to the equation indicated; [e]: *F*-value for the indicated comparison; [f]: critical *F*-value for $a=0.05$; [g]: coefficients of variation, in percent (estimated by the nonlinear regression software).

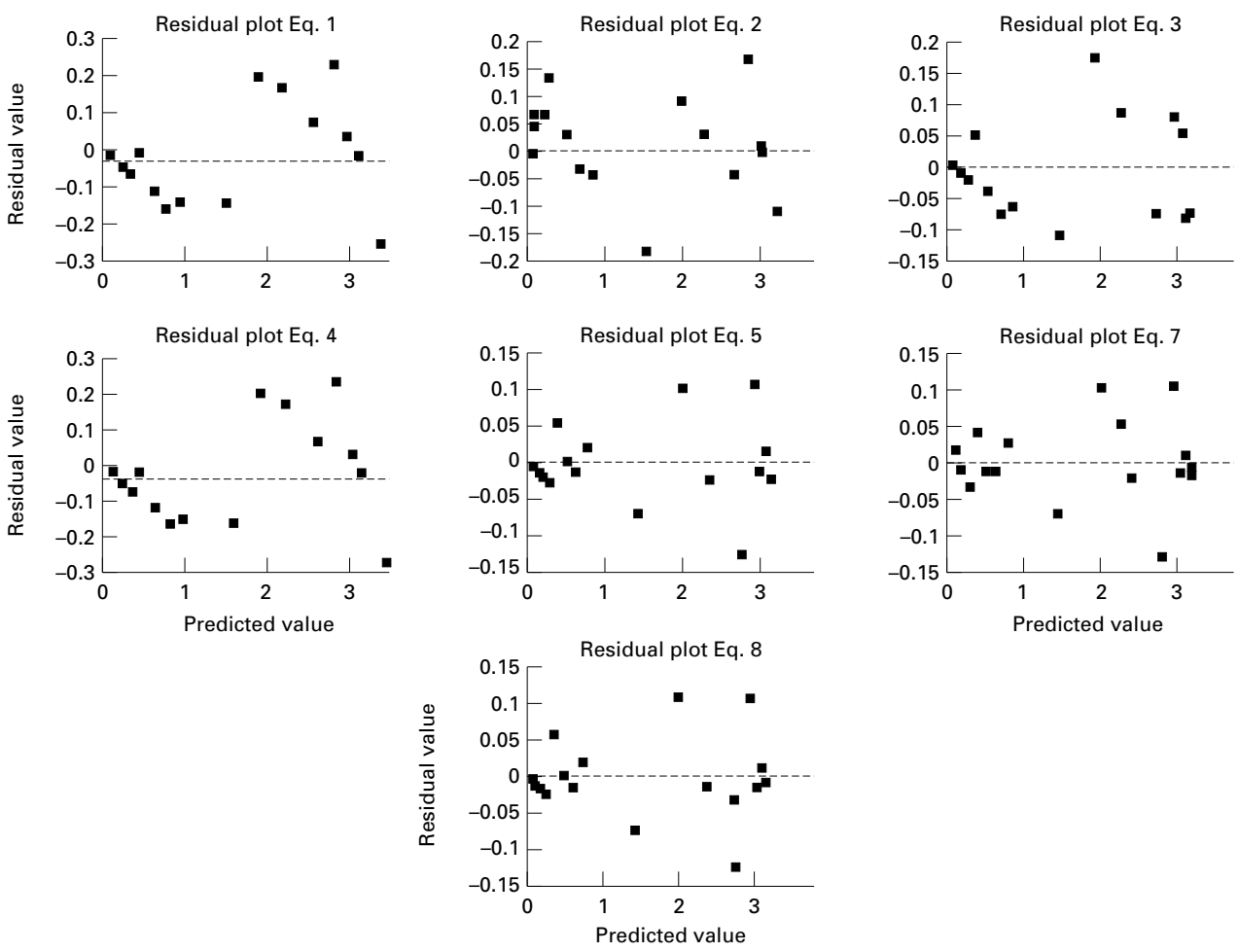

Figure 2 Residual plots for the iterations of model-equations 1–5, 7 and 8 of uninhibited NT-formation rates.

AIC, equation 8 was to be preferred. This is a model reflecting two enzymes, one with substrate inhibition and one with 'Hill-kinetics' (Table 4). The *F*-test showed that equation 6 fit better than the three parameter models. No further improvement was achieved with the six-parameter models. The residual plots of equations 6,

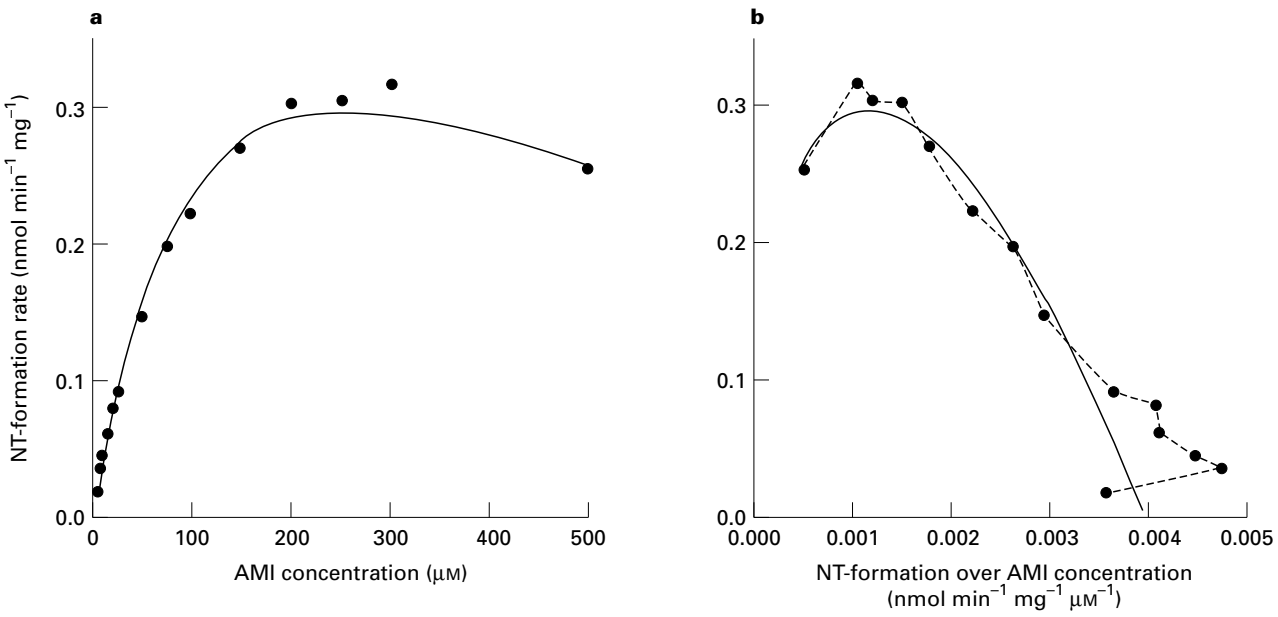

Figure 3 Plot of NT-formation rate *vs* AMI concentration (a) and Eadie-Hofstee plot (b) for NT-formation in presence of 10 μM KET. The solid line in both graphs represents the curve of best fit as iterated with equation 3. The broken line joins the points with respect to increasing substrate concentration.

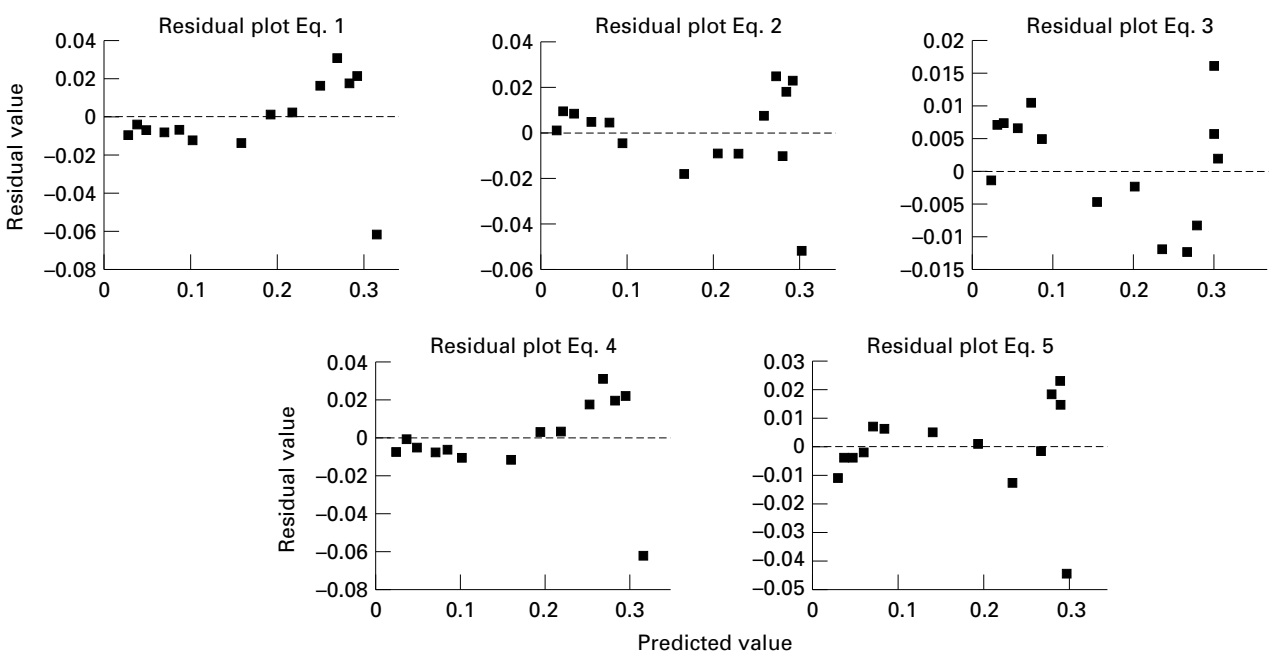

Figure 4 Residual plots for the iterations of model-equations 1–5 of NT-formation rates in presence of 10 μM KET.

and 8 appeared to be randomly distributed (Figure 9). Equation 7 did not yield a convergent solution.

Coefficients of variation (CV), determined as the standard error divided by the parameter estimate (percent) as provided by the iterative computer program [17], were 30% for equations 1–3, between 400 and $>10^6$ for equation 4. With regard to the favoured equations, CV were smaller than 200% for AMI without inhibitor, smaller than 30% for AMI with KET, smaller than 90% for AMI with SPA, and very high for AMI with KET and SPA for equation 8 with a CV up to 2500% but smaller than 100% for equation 6.

Discussion

Many metabolic pathways are mediated by more than one CYP enzyme, and reciprocal plots (e.g., Eadie-Hofstee or Lineweaver-Burk plot) often provide evidence that single enzyme MM kinetics are not applicable for a particular pathway [21]. In addition, fitting data with a model equation not reflecting the 'true' distribution of the data points yields interdependent residual errors which deviate from a normal distribution with a non-zero mean [22].

The NT formation rate profile displayed a convex

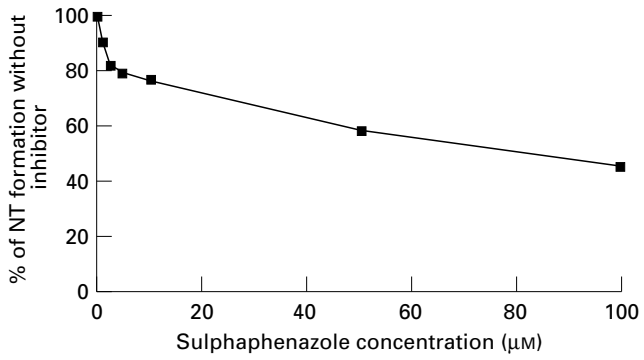

Figure 5 Dependency of NT-formation on varying concentration of the CYP2C9 inhibitor sulphaphenazole with a fixed AMI concentration of 100 μM. Points represent the reaction velocity with that concentration of inhibitor present relative to the velocity without inhibitor.

pattern in the scattering of the data points in the Eadie Hofstee plot. Therefore NT formation was not consistent with a single (equation 1) or double MM equation (equation 4). Instead a model was required that integrates a sigmoidal shape in the constructed curve. Such a model is the Hill equation for cooperative substrate binding (equation 2). It reflects a setting in which binding sites can cooperate with each other [23] and where the coefficient n represents the degree of cooperativity. CYP3A3/4 is known to exhibit cooperativity [5, 14, 24, 25], and there is evidence for binding of two substrate molecules in the CYP3A3/4 active site [26]. Lack of increase in velocity with increasing substrate concentrations could also be interpreted as inhibition by substrate. Such a condition is expressed by equation 3. Equations 1 to 6 were applied to a NT

Table 2 Kinetic parameters and statistical evaluation of NT formation in presence of 10 μM KET

Model	V_{max}[a]	K_m[a]; K'[a]	n[a]; K_1[a]	V_{max}[b]	K_m[b]; K'[b]	n[b]; K_1[b]	*AIC*[c]	*Comp.*[d]	F[e]	$F_{\{0.05\}}$[f]
Eq. 1	0.35	61					−66.7	Eq. 2	3.6	4.75
								Eq. 3	61.7	4.75
CV[g]	6	19								
Eq. 2	0.32	47	1.32				−68.7	Eq. 5	1.8	4.1
CV[g]	6.8	18	16							
Eq. 3	0.74	186	0.0028				−91.1	Eq. 5	−3.2[h]	4.1
CV[g]	16	22	30							
Eq. 4	0.09	61		0.27	61		−62.7			
CV[g]	$>10^6$	$>10^6$		$>10^6$	$>10^6$					
Eq. 5	0.14	19		0.16	73	2.89	−69.4			
CV[g]	139	218		109	21	87				

Equations 6–8 did not yield a convergent solution. Equation 4 was not included in the comparison with the *F*-test because it provided values for the sum of squared residuals which were identical as for equation 1. V_{max} in nmol min^{-1} mg^{-1} protein; K_m, K' in μM; K_1 in μM^{-1}; n arbitrary units; [a]: first enzyme; [b]: second enzyme; [c]: Akaike's information criterion; [d]: comparison to the equation indicated; [e]: *F*-value for the indicated comparison; [f]: critical *F*-value for $a=0.05$; [g]: coefficients of variation, in percent (estimated by the nonlinear regression software); [h]: a negative value for *F* indicates that the sum of squared residuals of the model with the higher number of parameters is greater than the sum of squared residuals for the model with fewer parameters.

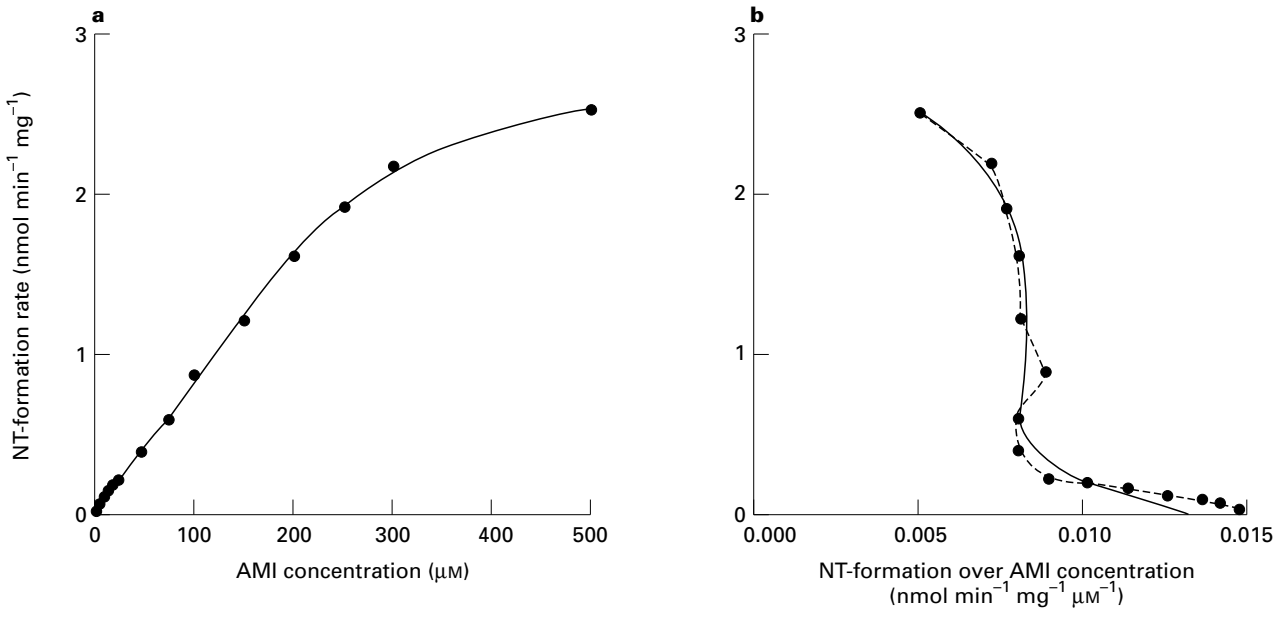

Figure 6 Plot of NT-formation rate *vs* AMI concentration (a) and Eadie-Hofstee plot (b) for NT-formation rates in presence of 50 μM SPA. The solid line in both graphs represents the curve of best fit as iterated with equation 5. The broken line joins the points with respect to increasing substrate concentration.

Table 3 Kinetic parameters and statistical evaluation of NT formation in presence of 50 μM SPA

Model	V_{max}[a]	K_m[a]; K'[a]	n[a]; K_1[a]	V_{max}[b]	K_m[b]; K'[b]	n[b]; K_1[b]	*AIC*[c]	*Comp.*[d]	F[e]	$F_{\{0.05\}}$[f]
Eq. 1	4.9	431					−31.2	Eq. 2	9.5	4.75
CV[g]	9.6	16								
Eq. 2	3.4	221	1.32				−38.0	Eq. 5	22	4.1
CV[g]	8.8	15	8.1							
Eq. 4	1.8	431		3.1	431		−27.2			
CV[g]	810	1325		460	753					
Eq. 5	0.7	54		2.1	195	2.38	−59.3	Eq. 7	0.2	5.12
								Eq. 8	0.9	5.12
CV[g]	66	86		23	4.4	17				
Eq. 7	0.9	81.6	0.9	1.9	194	2.41	−57.6			
CV[g]	388	624	69	132	8.7	54				
Eq. 8	1.2	108.0	0.0017	2.1	217	2.51	−58.8			
CV[g]	161	153	14030	2020	179	432				

Equations 3 and 6 did not yield a convergent solution. Equation 4 was not included in the comparison with the *F*-test because it provided values for the sum of squared residuals which were identical as for equation 1. V_{max} in nmol min^{-1} mg^{-1} protein; K_m, K' in μM; K_1 in μM^{-1}; n arbitrary units; [a]: first enzyme; [b]: second enzyme; [c]: Akaike's information criterion; [d]: comparison to the equation indicated; [e]: *F*-value for the indicated comparison; [f]: critical *F*-value for $a=0.05$; [g]: coefficients of variation, in percent (estimated by the nonlinear regression software).

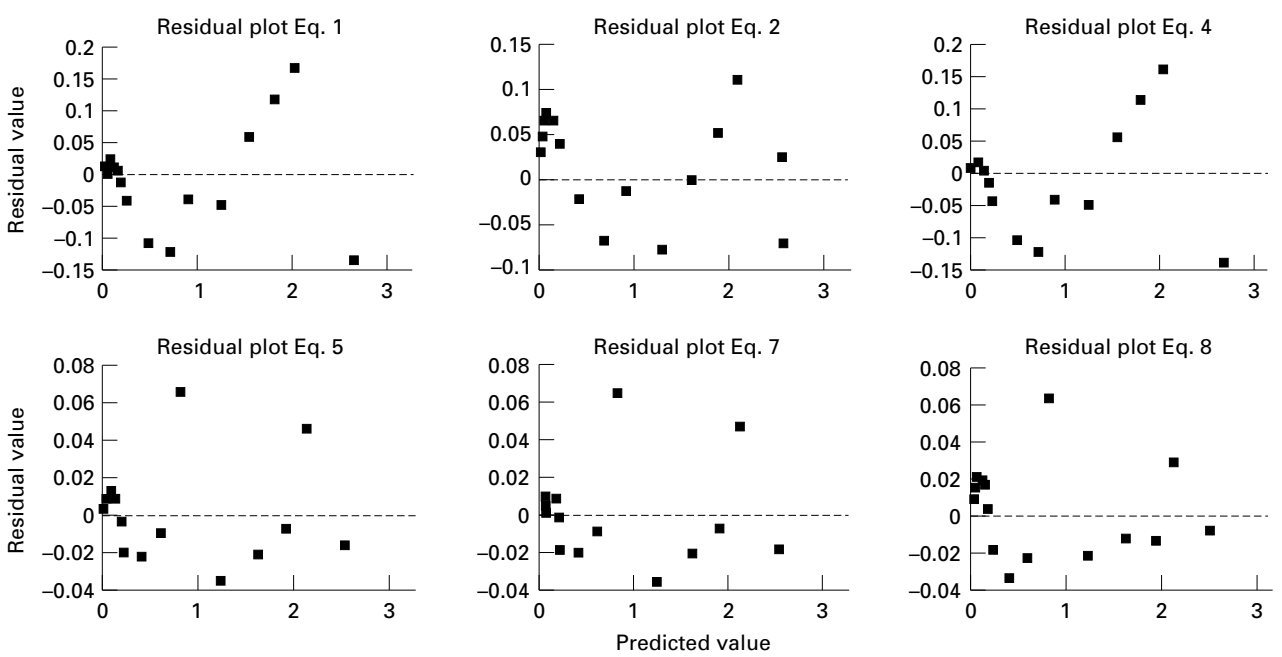

Figure 7 Residual plots for the iterations of model-equations 1–5, 7 and 8 of NT-formation rates in presence of 50 μM SPA.

formation rate *vs* AMI concentration curve with 15 data points, a larger number of data points than would usually be obtained, to allow fitting of more complex model equations with additional iterated parameters. The superiority of equation 5 was clearly indicated by the AIC and by the *F*-test (Table 1). The plots of residuals *vs* predicted values [10, 22] displayed an obvious improvement in the scattering of points of equation 5 *vs* equations 1–4, whereas the residual plot of equation 6 provided no further improvement. Therefore, a model consisting of a MM-enzyme and a Hill-enzyme appears to describe NT-formation with reasonable precision.

The finding that more than one enzyme is involved in this reaction is consistent with ongoing work in which we have found that the *N*-demethylation of AMI is mediated by CYP3A3/4 [5]. It is evident that at least one other enzyme is involved in this metabolism. A contribution of CYP1A1/2 and CYP2D6 to this reaction was effectively ruled out, since AMI-demethylation was not decreased by specific chemical inhibitors of these cytochromes [5].

Assuming that CYP3A3/4 accounts for the 'sigmoidal part' of Figure 1 in a two enzyme pathway, abolishing CYP3A3/4 activity should result in residual demethylase activity conforming to single MM kinetics. The Eadie Hofstee plot of the NT formation rates in presence of KET is consistent with this hypothesis (Figure 3b). At 500 μM however, a decrease in AMI demethylation rate was observed (Figure 3a), as typically occurs in the case of substrate or product inhibition. Equation 3 achieves the lowest AIC, and the introduction of additional

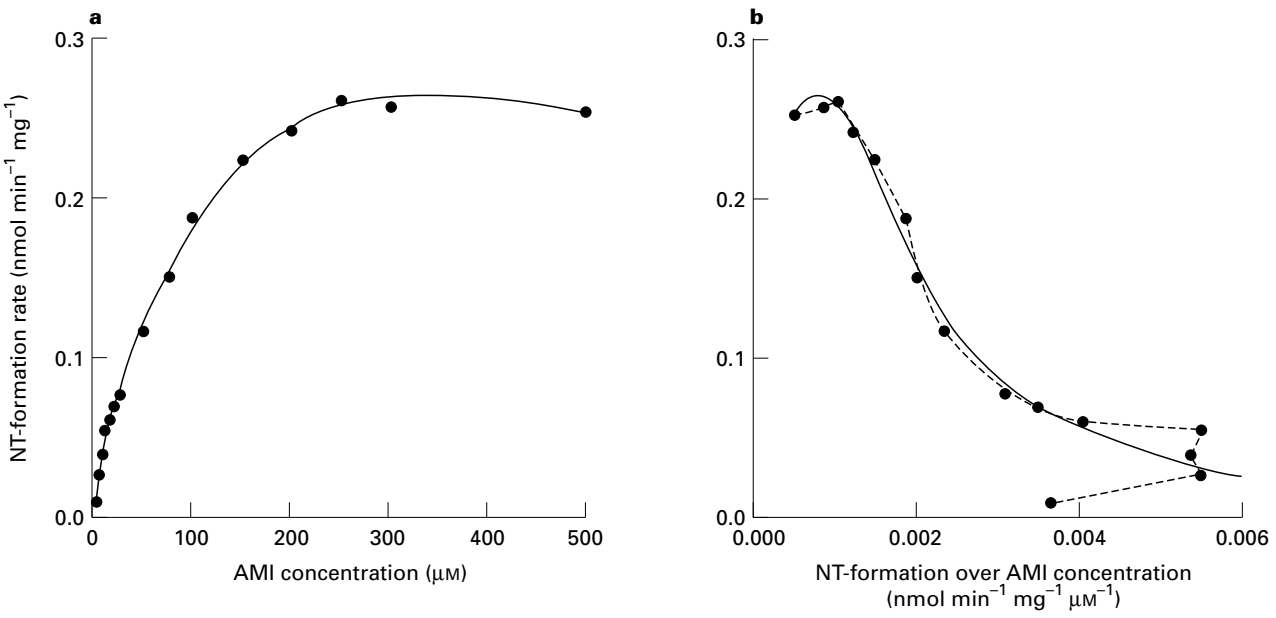

Figure 8 Plot of NT-formation rate *vs* AMI concentration (a) and Eadie-Hofstee plot (b) for NT-formation rates in presence of 10 μM KET and 50 μM SPA. The solid line in both graphs represents the curve of best fit as iterated with equation 6. The broken line joins the points with respect to increasing substrate concentration.

Table 4 Kinetic parameters and statistical evaluation of NT formation in presence of 10 μM KET and 50 μM SPA

Model	V_{max}[a]	K_m[a]; K'[a]	n[a]; K_1[a]	V_{max}[b]	K_m[b]; K'[b]	n[b]; K_1[b]	*AIC*[c]	*Comp.*[d]	F[e]	$F_{\{0.05\}}$[f]
Eq. 1	0.3	68					−91.6	Eq. 2	−0.01[h]	4.75
								Eq. 3	5.1	4.75
CV[g]	3.6	11								
Eq. 2	0.3	69	0.99				−89.6	Eq. 5	−4.2[h]	4.1
								Eq. 6	22.5	4.1
CV[g]	7.6	21	11							
Eq. 3	0.4	98	0.0006				−94.9	Eq. 5	−4.4[h]	4.1
								Eq. 6	14.4	4.1
CV[g]	11	19	55							
Eq. 4	0.1	68		0.3	68		−87.6			
CV[g]	1445	4406		347	1057					
Eq. 5	0.13	17		0.1	93	3.12	−58.8	Eq. 8	446	5.12
CV[g]	22	39		21	6.3	22				
Eq. 6	0.05	7.0		0.8	443	0.0041	−111.1	Eq. 8	4.9	5.12
CV[g]	53	89		55	84	92				
Eq. 8	0.12	16.5	0.0020	0.2	105	2.36	−115.6			
CV[g]	25	38	2495	401	54	132				

Equation 7 did not yield a convergent solution. Equation 4 was not included in the comparison with the *F*-test because it provided values for the sum of squared residuals which were identical as for equation 1. V_{max} in nmol min^{-1} mg^{-1} protein; K_m, K' in μM; K_1 in μM^{-1}; n arbitrary units; [a]: first enzyme; [b]: second enzyme; [c]: Akaike's information criterion; [d]: comparison to the equation indicated; [e]: *F*-value for the indicated comparison; [f]: critical *F*-value for $a=0.05$; [g]: coefficients of variation, in percent (estimated by the nonlinear regression software); [h]: a negative value for *F* indicates that the sum of squared residuals of the model with the higher number of parameters is greater than the sum of squared residuals for the model with fewer parameters.

parameters does not improve the quality of fit according to the *F*-test (Table 2). However, the parameters do not match those derived for the MM kinetic component of the formation rate curve without inhibitor. The concentration of KET was 10 μM, which should abolish all CYP3A3/4 activity. However, KET may produce some degree of inhibition of other CYP isoforms at this concentration [27]. Previous reports provide evidence that the *N*-demethylation of AMI co-segregates with S-mephenytoin 4′-hydroxylation [28, 29], a CYP2C19 mediated reaction [30, 31]. However, a polyclonal goat anti rat CYP2C11 antibody did not substantially affect NT formation in this liver sample. It did inhibit 4′-hydroxy-mephenytoin formation in microsomes of this same liver tissue by 66% [6]. Thus, CYP2C19 is unlikely to contribute to any significant extent to this reaction. In contrast, SPA, a specific CYP2C9 inhibitor [27, 32], displayed a concentration-dependent inhibition

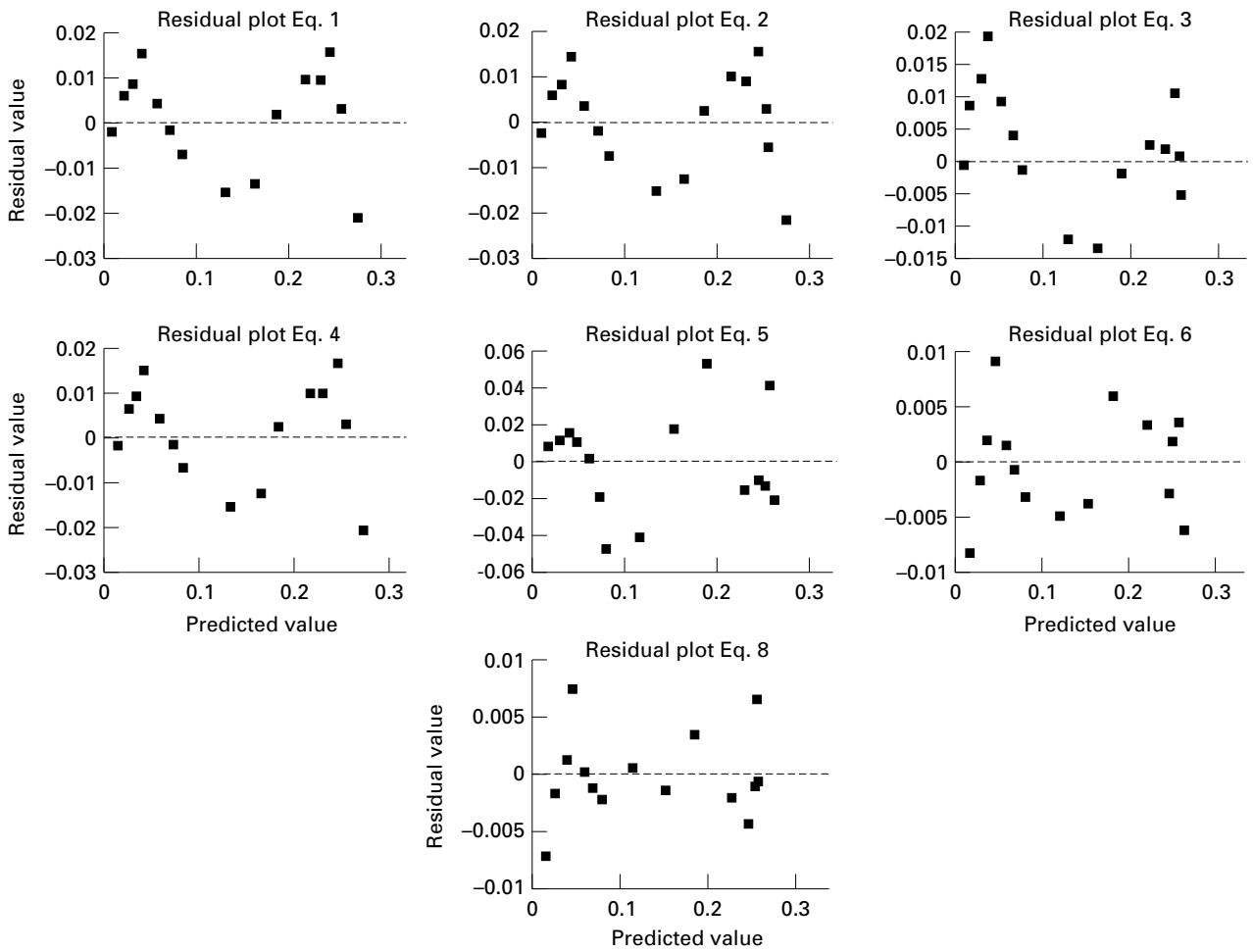

Figure 9 Residual plots for the iterations of model-equations 1–8 of NT-formation rates in presence of 10 μM KET and 50 μM SPA.

of AMI *N*-demethylation (Figure 5), indicating that SPA decreased considerably but did not abolish CYP2C9 contributes substantially to this reaction.

Incubating a fixed concentration of 50 μM SPA (a concentration likely to inhibit all CYP2C9 activity [27]) with increasing concentrations of AMI resulted in a biphasic pattern of the formation rate (Figures 6a, b), with a convex-shaped low-affinity site and a linear high-affinity site. This plot and the *F*-test and AIC analysis (Table 3) are consistent with the presence of a low-affinity Hill-enzyme and a high affinity MM-enzyme. Values for V_{max} and the Hill-coefficient were in the same range as the parameters for the 'Hill-enzyme' as iterated for the NT-formation rate curve without inhibitor, whereas K' was different by a factor of 2.8 (Tables 1 and 3). Thus, it is likely that the Hill-enzyme is unaffected by SPA. However, the difference in K' might be attributable to the presence of the inhibitor, although SPA is reported to be relatively specific for CYP2C9. One should also consider that the iterative process is sensitive to slight changes in observed values (e.g., rounding) especially with the application of multiple parameter models.

Because two sites of AMI *N*-demethylation could be identified, despite the presence of SPA (assuming complete inhibition of CYP2C9), at least three different enzymes are evidently involved in this pathway. Removing CYP3A3/4 and CYP2C9 activity by incubation of AMI with fixed concentrations of KET and NT-formation rates. The complex shape of the resulting Eadie-Hofstee plot indicated the need for a multi parameter model. A small decrease in velocity at high substrate concentrations suggested substrate inhibition and the slightly concave curvature might be attributable either to a high and low affinity site or to variance in the observed data points. This variance is exaggerated for small substrate concentrations in the Eadie-Hofstee plot. The model of an enzyme with substrate inhibition and an enzyme with Hill-kinetics was suggested by AIC (Table 4). The *F*-test supported equation 6, modelling the combination of a MM-enzyme and a substrate inhibited enzyme. Since equation 8 was not superior to equation 6 based on the *F*-test, and the residuals were fairly randomly scattered, we favour the simpler (fewer parameter) model (equation 6) to describe these data points.

AMI *N*-demethylation appears to be mediated by more than one enzyme, one of which reflects allosteric kinetics. The only CYP activity known to date to be consistent with such kinetics is CYP3A3/4. KET eliminated allosteric enzyme activity and the remaining NT-formation was best described by modelling substrate inhibition. However, the contribution of an enzyme with such kinetic properties to NT-formation was not consistent with the modelling of AMI *N*-demethylation without inhibitor. It is possible that KET, a strong but

nonspecific CYP3A3/4 inhibitor, may have modified the remaining *N*-demethylase activity as would be the case for a substrate inhibited enzyme. It is also possible that NT-formation at concentrations of AMI (without inhibitor) higher than those that we tested (>500 μM) may have become attenuated, thereby suggesting a model that includes substrate inhibition. Our previous study of NT-formation from AMI, although based on a smaller number of data points, suggested substrate inhibition at higher AMI concentrations [5]. SPA, a CYP2C9 inhibitor of relative high specificity, reduced maximal NT-formation (V_{max}) by approximately 16% and the remaining demethylase activity appeared to be composed of two enzymes (Hill and MM).

The results of NT-formation in presence of KET and SPA are difficult to interpret, since both inhibitors might modify the activity of the remaining *N*-demethylation mediating enzymes. The remaining *N*-demethylase activity appeared to be best described by a two MM enzyme model, one with and one without substrate inhibition.

In summary a combination of enzyme kinetic modelling and experimental data have allowed the further characterisation of the *N*-demethylation of AMI *in vitro*. It appears that at least three different enzymes, and possibly four, contribute to this reaction. Two enzymes have been identified as CYP3A3/4 and CYP2C9 with reasonable certainty although further work in several more livers is required to confirm the participation of CYP2C9. There is evidence to suggest that CYP2C19 also contributes to this reaction [28, 29], although the results of immunoinhibition with the rat liver CYP2C11 antibody did not confirm the participation of CYP2C19 in the liver sample studied. Considering the apparently small relative contribution of this enzyme to NT-formation (<20 % at a concentration of 100 μM AMI, as calculated with the iterated parameters for this liver sample) and the limited inhibitory capacity of the utilized antibody [6], a small contribution CYP2C19 activity is likely to remain undetected with this assay.

AMI *N*-demethylation involves several enzymes with different underlying reaction mechanisms. At low substrate concentrations of AMI *N*-demethylation appears to be mediated mainly by the high affinity but low capacity enzymes with MM characteristics (tentatively CYP2C9 and possibly CYP2C19). With increasing AMI concentrations, however, the relative contribution of the low affinity, high capacity enzyme, which is CYP3A3/4, increases rapidly due to its allosteric property.

Human CYP3A3/4 appears to possess a broad spectrum of substrates which belong to different classes of chemicals, and which catalyze a variety of different reactions (dealkylation, hydroxylation, nitroreduction). For some of these substrates allosteric kinetics have been reported [14, 24, 25]. However, only a few drugs are metabolised solely by CYP3A3/4 [9, 33, 34] and to date no *in vivo* index reaction for this cytochrome is clearly established. It appears that human liver tissue contains a variety of relatively specific high affinity cytochrome P450, but of limited capacity. Once the substrate concentration exceeds the capacity of high-affinity, low-capacity enzymes, nonlinear kinetics are predicted, which may predispose to clinical toxicity. It is possible that such situations are often prevented by an increasing relative contribution of CYP3A3/4. Thus CYP3A3/4 may function as physiologic 'backup' enzyme. This might also explain why CYP3A3/4 is the most abundant CYP found in human liver [35].

This work was supported by Grant MH-34223 from the Department of Health and Human Services. Dr Schmider is the recipient of a Merck, Sharp & Dohme International Fellowship in Clinical Pharmacology.

1 Warner M, Gustafsson JA. Extrahepatic microsomal forms: brain cytochrome P450. In *Cytochrome P450*. eds Schenkman JB, Greim H, Berlin: Springer Verlag, 1993: 387–97.

2 Kolars JC, Schmiedlin-Ren P, Schuetz JD, Fang C, Watkins PB. Identification of rifampin-inducible P450IIIA4 (CYP3A4) in human small bowel enterocytes. *J Clin Invest* 1992; **90**: 1871–1878.

3 Kolars JC, Awni WC, Merion RM, Watkins PB. First-pass metabolism of cyclosporin by the gut. *Lancet* 1991; **338**: 1488–1490.

4 Herbert MF, Roberts JP, Prueksaritanont T, Benet LZ. Bioavailability of cyclosporine with concomitant rifampicin administration is markedly less than predicted by hepatic enzyme induction. *Clin Pharmacol Ther* 1992; **52**: 453–457.

5 Schmider J, Greenblatt DJ, von Moltke LL, Harmatz JS, Shader RI. *N*-demethylation of amitriptyline *in vitro*: role of cytochrome P-450 3A (CYP3A) isoforms, and effect of metabolic inhibitors. *J Pharmacol Exp Ther* 1995; **275**: 592–597.

6 Schmider J, Greenblatt DJ, von Moltke LL, Harmatz JS, Duan SX, Karsov D, Shader RI. Characterization of six *in vitro* reactions mediated by human cytochrome P450: application to the testing of cytochrome P450 directed antibodies. *Pharmacology* 1996; **52**: 125–134.

7 Schmider J, Greenblatt DJ, von Moltke LL, Harmatz JS, Shader RI. Inhibition of cytochrome P450 by nefazodone *in vitro*: studies of dextromethorphan *O*- and *N*-demethylation. *Br J Clin Pharmacol* 1996; (in press).

8 von Moltke LL, Greenblatt DJ, Harmatz JS, Shader RI. Cytochromes in psychopharmacology. *J Clin Psychopharmacol* 1994; **14**: 1–4.

9 von Moltke LL, Greenblatt DJ, Cotreau-Bibbo MM, Harmatz JS, Shader RI. Inhibitors of alprazolam metabolism *in vitro*: effect of serotonin-reuptake-inhibitor antidepressants, ketoconazole and quinidine. *Br J Clin Pharmacol* 1994; **38**: 23–31.

10 Motulsky HJ, Ransnas LA. Fitting curves to data using nonlinear regression: a practical and nonmathematical review. *FASEB J* 1987; **1**: 365–374.

11 Boxenbaum HG, Riegelman S, Elashoff RM. Statistical estimations in pharmacokinetics. *J Pharmacokin Biopharm* 1974; **2**: 123–148.

12 Akaike H. An information criterion (AIC). *Math Sci* 1976; **14**: 5–9.

13 Yamaoka K, Nakagawa T, Uno T. Application of Akaike's information criterion (AIC) in the evaluation of linear pharmacokinetic equations. *J Pharmacokin Biopharm* 1978; **6**: 165–175.

14 von Moltke LL, Greenblatt DJ, Harmatz JS, Shader RI. Alprazolam metabolism in vitro: studies of human, monkey, mouse, and rat liver microsomes. *Pharmacology* 1993; **47**: 268–276.

15 von Moltke LL, Greenblatt DJ, Cotreau-Bibbo MM,

Duan SX, Harmatz JS, Shader RI. Inhibition of desipramine hydroxylation *in vitro* by serotonin-reuptake-inhibitor antidepressants, and by quinidine and ketoconazole: a model system to predict drug interactions *in vivo*. *J Pharmacol Exp Ther* 1994; **268**: 1278–1283.

16 Halvorson M, Greenway D, Eberhart D, Fitzgerald K, Parkinson A. Reconstitution of testosterone oxidation by purified rat cytochrome P450p (IIIA1). *Arch Biochem Biophys* 1990; **277**: 166–180.

17 Norby J, Rubenstein S, Tuerke T, Farmer S, Forood R, Bennington J. *SigmaPlot*, *v. 4.13*. Jandel Corporation 1991.

18 Mannervik B. Design and analysis of kinetic experiments for discrimination between rival models. In *Kinetic data analysis*. eds Endrenyi L, New York: Plenum Press, 1981: 235–270.

19 Cornish-Bowden A. *Principles of enzyme kinetics*. London–Boston: Butterworths, 1976: 66–67.

20 Segel IH. *Enzyme kinetics*: *behavior and analysis of rapid equilibrium and steady state enzyme systems*. New York: Wiley & Sons, Inc., 1975: 346–462.

21 Bardsley WG, Leff P, Kavanagh J, Waight RD. Deviations from Michaelis-Menten kinetics. The possibility of complicated curves for simple kinetic schemes and the computer fitting of experimental data for acetylcholinesterase, acid phosphatase, adenosine deaminase, arylsulphatase, benzylamine oxidase, chymotrypsin, fumarase, galactose dehydrogenase, beta-galactosidase, lactate dehydrogenase, peroxidase and xanthine oxidase. *Biochem J* 1980; **187**: 739–765.

22 Jeng YJ, Martin A. Residuals in multiple regression analysis. *J Pharm Sci* 1985; **74**: 1053–57.

23 Pratt WB, Taylor P. *Principles of drug action*. 3rd edition. Eds Pratt WB, Taylor P. New York, Edinburgh, London, Melbourne: Churchill Livingstone Inc., 1990: 54.

24 Andersson T, Miners JO, Veronese ME, Birkett DJ. Diazepam metabolism by human liver microsomes is mediated by both S-mephenytoin hydroxylase and CYP3A isoforms. *Br J Clin Pharmacol* 1994; **38**: 131–137.

25 Schwab GE, Raucy JL, Johnson EF. Modulation of rabbit and human hepatic cytochrome P-450-catalyzed steroid hydroxylations by alpha-naphthoflavone. *Mol Pharmacol* 1988; **33**: 493–499.

26 Shou M, Grogan J, Mancewicz JA, *et al*. Activation of CYP3A4: evidence for the simultaneous binding of two substrates in a cytochrome P450 active site. *Biochemistry* 1994; **33**: 6450–6455.

27 Newton DJ, Wang RW, Lu AYH. Cytochrome P450 inhibitors. Evaluation of specificities in the *in vitro* metabolism of therapeutic agents by human liver microsomes. *Drug Metab Dispos* 1995; **23**: 154–158.

28 Baumann P, Jonzier-Perey M, Koeb L, Küpfer A, Tinguely D, Schopf J. Amitriptyline pharmacokinetics and clinical response: II. Metabolic polymorphism assessed by hydroxylation of debrisoquine and mephenytoin. *Int Clin Psychopharmacol* 1986; **1**: 102–112.

29 Breyer-Pfaff U, Pfandl B, Nill K, *et al*. Enantioselective amitriptyline metabolism in patients phenotyped for two cytochrome P450 isozymes. *Clin Pharmacol Ther* 1992; **52**: 350–358.

30 Goldstein JA, Faletto MB, Romkes-Sparks M, *et al*. Evidence that CYP2C19 is the major (S)-mephenytoin 4′-hydroxylase in humans. *Biochemistry* 1994; **33**: 1743–1752.

31 Wrighton SA, Stevens JC, Becker GW, VandenBranden M. Isolation and characterization of human liver cytochrome P450 2C19: correlation between 2C19 and S-mephenytoin 4′-hydroxylation. *Archiv Biochem Biophys* 1993; **306**: 240–245.

32 Baldwin SJ, Bloomer JC, Smith GJ, Ayrton AD, Clarke SE, Chenery RJ. Ketoconazole and sulphaphenazole as the respective selective inhibitors of P4503A and 2C9. *Xenobiotica* 1995; **25**: 261–270.

33 Kronbach T, Mathys D, Umeno M, Gonzalez FJ, Meyer UA. Oxidation of midazolam and triazolam by human liver cytochrome P450IIIA4. *Mol Pharmacol* 1989; **36**: 89–96.

34 Hunt CM, Westerkam WR, Stave GM. Effect of age and gender on the activity of human hepatic CYP3A. *Biochem Pharmacol* 1992; **44**: 275–283.

35 Shimada T, Yamazaki H, Mimura M, Inui Y, Guengerich FP. Interindividual variations in human liver cytochrome P-450 enzymes involved in the oxidation of drugs, carcinogens and toxic chemicals: studies with liver microsomes of 30 Japanese and 30 Caucasians. *J Pharmacol Exp Ther* 1994; **270**: 414–23.

(*Received 9 August 1995, accepted 25 January 1996*)